Journal of Solid State Chemistry 184 (2011) 2458–2461

Contents lists available at ScienceDirect

Journal of Solid State Chemistry

journal homepage: www.elsevier.com/locate/jssc

Two types of diffusions at the cathode/electrolyte interface in IT-SOFCs

Zhi-Peng Li [a,*], Toshiyuki Mori [a], Graeme John Auchterlonie [b], Jin Zou [b,c], John Drennan [b]

[a] Global Research Center for Environment and Energy based on Nanomaterials Science, National Institute for Materials Science, Tsukuba, Ibaraki 305-0044, Japan
[b] Centre for Microscopy and Microanalysis, The University of Queensland, St. Lucia, Brisbane, Queensland 4072, Australia
[c] Division of Materials, The University of Queensland, St. Lucia, Brisbane, Queensland 4072, Australia

ARTICLE INFO

Article history:
Received 13 June 2011
Received in revised form
12 July 2011
Accepted 13 July 2011
Available online 22 July 2011

Keywords:
Grain boundary
Interdiffusion
Interface
Scanning transmission electron microscopy
Segregation
Solid oxide fuel cell

ABSTRACT

Analytical transmission electron microscopy, in particular with the combination of energy dispersive X-ray spectroscopy (EDX) and electron energy-loss spectroscopy (EELS), has been performed to investigate the microstructure and microchemistry of the interfacial region between the cathode ($La_{0.6}Sr_{0.4}Co_{0.8}Fe_{0.2}O_3$, LSCF) and the electrolyte (Gd-doped ceria, GDC). Two types of diffusions, mutual diffusion between cathode and electrolyte as well as the diffusion along grain boundaries, have been clarified. These diffusions suggest that the chemical stability of LSCF and GDC are not as good as previously reported. The results are more noteworthy if we take into consideration the fact that such interdiffusions occur even during the sintering process of cell preparation.

1. Introduction

The high operating temperature of solid oxide fuel cells (SOFCs), i.e. 900–1000 °C, usually results in complex problems, such as cell degradation, difficulties in materials selection and other cost-effect issues [1,2]. This motivates the efforts to decrease the operating temperature to intermediate temperatures (500–700 °C). One dilemma facing the intermediate temperature SOFCs (IT-SOFCs) application is the sintering temperature of ceramics cell components. As for the compromise, the sintering temperature should be neither too low to synthesize a fully dense electrolyte, nor too high to lead to interactions or interdiffusions among constituent species. For instance, the reaction between zirconia electrolyte and $La_{1-x}Sr_xMnO_3$ cathode can lead to the insulating layer (e.g., $La_2Zr_2O_7$ or $SrZrO_3$) formation at the cathode/electrolyte interface [3,4]. These low conductivity zirconates, or other secondary phases formed are revealed as the predominant reason for cell degradation. It is also known that even small amounts of segregated dopants/impurities at the electrode/electrolyte interface can alter the properties of SOFC materials, and consequently result in a decrease in durability and even the overall performance of the system [5]. Therefore, the interactions or interdiffusions among cell components should be avoided by all means. As a consequence, the interfacial barrier layer is put forward to mitigate the insulating layer or impurity phase formation between the electrode and the electrolyte [6]. Owing to the good stability to La-based perovskite cathode materials, e.g., $La_{1-x}Sr_xCoO_3$ or $La_{1-x}Sr_xCo_{1-y}Fe_yO_3$ (LSCF), Gd-doped ceria (GDC) is regarded as a potential candidate for the interfacial barrier layer or as an alternative electrolyte material for IT-SOFCs [7,8]. It has been reported that the GDC interlayers between cathode and electrolyte can inhibit interdiffusion and consequently improve the electrochemical performance of IT-SOFCs [6,9].

Note that, even though it is for IT-SOFC cell fabrication, high fabrication temperature is generally inevitable. Moreover, the recent investigations have illustrated that mutual diffusion can take place at the anode/electrolyte interface as well as at the anode site of the Ni/GDC and Ni/Sm-doped ceria materials systems, during the sintering process of IT-SOFC sample preparation [10–12]. Hence, it is essential to investigate in more detail the possible diffusions at the interface between LSCF cathode and GDC electrolyte, in spite of their reported good chemical stability. More specifically, characterizing the diffusion phenomenon helps to generate fundamental knowledge on the local chemistry, element spatial distribution and related mechanism that is vital for the development of high-quality electrode/electrolyte interface. In this study, the interface between the LSCF cathode and the GDC electrolyte of a half-cell sample was characterized not only by electron microscopy for imaging, but also by the analytical TEM that can perform extensive micro-analytical investigations, and generate chemical composition and electronic structure information.

* Corresponding author. Fax: +81 29 8604712.
E-mail address: LI.Zhipeng@nims.go.jp (Z.P. Li).

0022-4596/$ - see front matter © 2011 Elsevier Inc. All rights reserved.
doi:10.1016/j.jssc.2011.07.021

2. Experimental

The ammonium carbonate co-precipitation method was applied to synthesize the electrolyte GDC nanopowders [13]. Cathode thin film was fabricated on GDC substrate by screen printing. The commercial raw $La_{0.6}Sr_{0.4}Co_{0.8}Fe_{0.2}O_3$ powders were mixed with 5.68 wt% Avicel (pore-forming agent), 1.14 wt% ethyl cellulose (binder), and 36.37 wt% terpineol (solvent). Such mixture was ball milled for 12 h to obtain homogeneous slurry, which was then screen printed onto the GDC sintered tablet. Two-step sintering was conducted for the screen printed sample: below 500 °C, the heating rate is as slow as 2 °C/min, and increased to 5 °C/min above 500 °C, till to target sintering temperature 1100 °C. The assembled sample was then sintered at 1100 °C in air for 2 h. Microstructure characterizations of the cathode/electrolyte interfacial region were performed on both SEM (Hitachi S-5000) and STEM (FEI Tecnai F20, field emission gun) equipped with a Gatan image filter and a high-angle annular dark-field (HAADF) detector. For high spatial resolution, the energy dispersive X-ray spectroscopy (EDX) and electron energy-loss spectroscopy (EELS) analyses were conducted at STEM mode. The STEM is operating with an extraction voltage of 4200 V, gun lens setting 6 and spot size 8. The convergence angle and collections angles for STEM EELS were about 0.5 and 5 mrad, respectively. Owing to the nanoprobe in the STEM mode, EELS spectra can be acquired at a very small region, i.e. around 5 nm, with sufficient beam intensity for micro-analyses. Therefore, STEM EELS analysis can be performed at different positions in this study, especially at grain boundaries and their nearby grain interiors. This can provide detailed information on local elements and electronic states, rather than the global information acquired by normal TEM EELS.

3. Results and discussion

The cross-sectional morphologies of LSCF cathode on GDC electrolyte are presented in Fig. 1. The image in Fig. 1(a) obtained by SEM displays that the porous thin film was well adhered on the dense substrate. Fig. 1(b) is a TEM bright field (BF) image, showing the similar morphology of the cathode/electrolyte interface. The interface can be easily recognized from the porous thin film and the dense substrate in the TEM image. For a quantitative analysis of the spatial distribution of constituent elements, the STEM EDX was performed across the interface. The corresponding concentration profiles are presented in Fig. 1(c). Note that the rare-earth elements Ce and Gd can diffuse from the electrolyte to the LSCF cathode. Simultaneously, the elements La, Sr, Co and Fe can also transport from the cathode to the GDC electrolyte through the interface. Moreover, all the elements have a similar diffusion length, indicating that substitution diffusion is the predominant mechanism, since there are significant differences in ionic radius among diffusing cations. Such mutual diffusion will consequently lead to a mutual diffusion zone (with an average 200 nm in width) formed at the cathode/electrolyte interface, similar to the diffusion phenomenon detected at the anode/electrolyte interface [10]. It is noteworthy that, contrary to the previous report that the insertion of lanthanum into fluorite ceria could be negligible [14], this mutual diffusion in LSCF/GDC materials cannot be neglected by any means.

In order to probe other possible diffusions occurring between the cathode and the electrolyte, further investigations have been conducted. Fig. 2 shows several contacted grains observed at the electrolyte side around the interface by STEM. In the STEM bright field (BF) image (Fig. 2(a)), two triple junctions (TJ), assigned as TJ1 and TJ2, can be clearly seen. It is interesting to note that there is a significant contrast difference between TJ1 and its

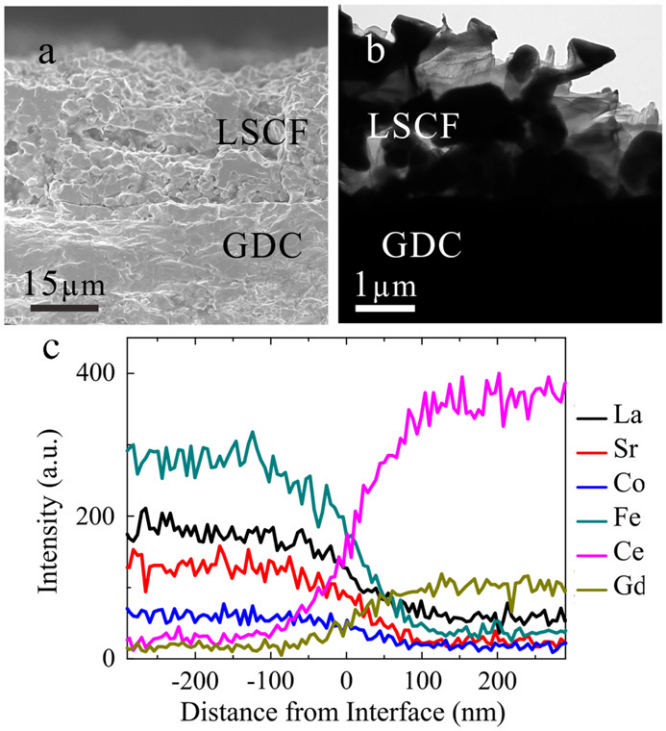

Fig. 1. Interfacial morphology between thin film cathode and electrolyte, characterized by (a) SEM and (b) TEM. (c) The concentration profile of STEM EDX line scan acquired across the cathode/electrolyte interface.

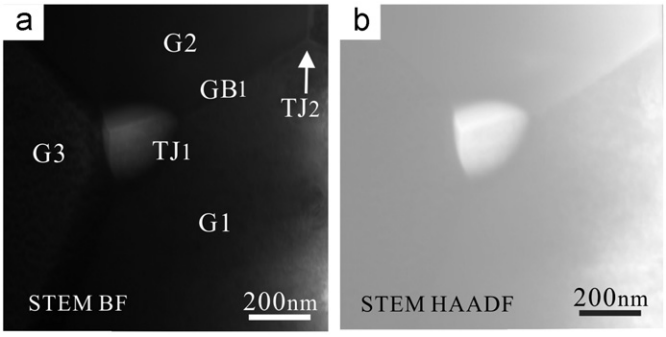

Fig. 2. Typical triple junctions, with different element segregation, observed at the electrolyte side around the cathode/electrolyte interface by STEM (a) BF and (b) HAADF, respectively.

neighboring areas. Such contrast difference is especially observable in the corresponding STEM HAADF image (Fig. 2(b)). Due to its varied sensitivity to different elements, the HAADF imaging is usually used as an intuitive way to distinguish the distribution of different elements based on contrast differences. Therefore, the special image of TJ1 shown in Fig. 2(a) may imply the segregation of different elements or impurities at this area. Analytical techniques were performed to verify such hypothesis.

In addition to the microstructural morphology at the interfacial region, the local chemical composition and electronic status are also needed. A series of STEM EDX spectra were recorded at grain interiors and boundaries of the same region shown in Fig. 2. From the corresponding spectra (Fig. 3), all the grains shown in Fig. 2 can be identified as GDC. Interestingly, besides the typical Ce and Gd peaks observed in grains 1, 2 and 3 (assigned as G1, G2 and G3 hereafter), an extra peak (marked by the arrow in Fig. 3) can be observed at the EDX spectrum acquired at TJ1, which is indexed as Lanthanum La peak. It is necessary to point out that,

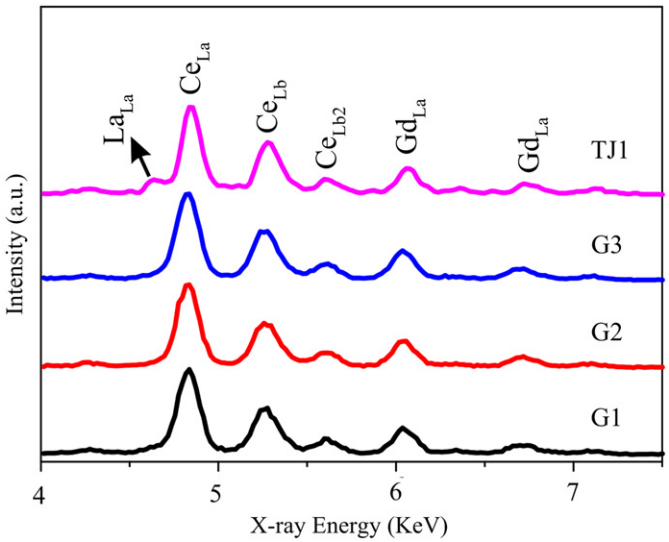

Fig. 3. STEM EDX results acquires at grain interiors, grain boundaries and triple junctions demonstrated in Fig. 2.

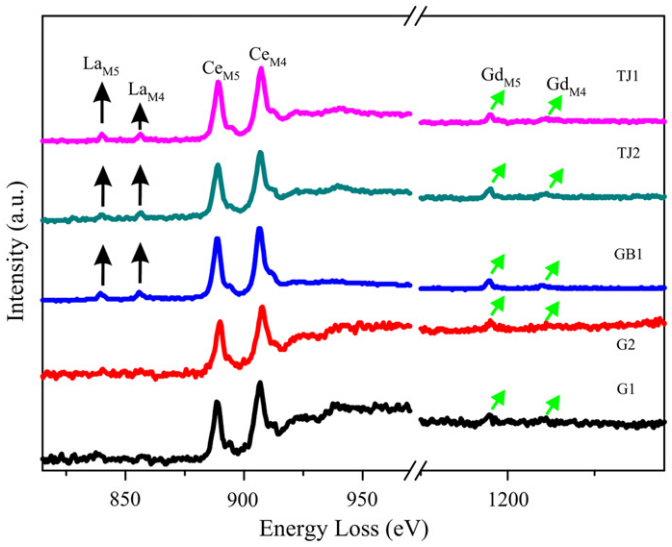

Fig. 4. Background subtracted STEM EELS spectra acquired at the grain interiors, triples junctions and the grain boundary listed in Fig. 2. (For interpretation of the references to color in this figure, the reader is referred to the web version of this article.)

during TEM sample preparation, the ion-milled powders from the LSCF-GDC sample will inevitably redeposit onto the sample surface and result in contaminations. If this were this case, powders with different elements would be homogeneously deposited onto sample surface. In other words, elements La, Sr, Co and Fe should be detected at all GDC regions, at both grain interiors and boundaries. Nevertheless, according to the systematic STEM EDX analyses, LSCF elements can only be detected around the cathode/electrolyte interfacial region, not in any other electrolyte parts. It is thereby inferred that such La peak in the EDX spectrum acquired at TJ1 may be attributed to the La diffusion from the LSCF side. Due to the limited precision of the current EDX technique that was caused by its intrinsic probe broadening and insufficient energy resolution, STEM EELS was used to explore the local element and associated concentration in more details at the same region shown in Fig. 2.

The STEM EELS spectra were acquired at the energy loss ranging from 800 to 1300 eV, where La–$M_{4,5}$, Ce–$M_{4,5}$ and Gd–$M_{4,5}$ adsorption edges can be recorded together. The STEM EELS results are demonstrated in Fig. 4. The characteristic adsorption peaks of different elements were extrapolated from the acquired spectra by subtracting the background following the power law fit. The spectra acquired at G1 and G2 (the black and red line in Fig. 4) illustrate that only Ce $M_{4,5}$ and Gd $M_{4,5}$ peaks (marked by green arrows) can be detected. However, in the spectrum acquired at TJ1 (the pink line in Fig. 4), extra peaks appeared (denoted by black arrows), indexed as La M_4 and M_5 peaks. Such La peaks can also be observed at the STEM EELS spectra acquired at the nearby triple junction TJ2 and the corresponding grain boundary connecting TJ1 and TJ2 (assigned as GB1 in Fig. 2). From all these spectra shown in Fig. 4, there are no visible differences in the intensity or energy shift of all the La, Ce and Gd peaks, implying that the local environment and bonding status of all the detected elements at grain boundaries or triple junctions are similar to that in grain interiors.

Besides the qualitative information about elements and related electronic status provided by the STEM EELS spectra, quantitative data about the concentrations of different elements can also be obtained by quantifying such spectra. The related quantification results are listed in Table 1. Note that La can only be detected in TJ1, TJ2 and GB1, but not in the neighboring grain interiors. Particularly, TJ1 has the highest La concentration, which is in accordance with the intuitive results in Fig. 2 that TJ1 has the strongest contrast difference compared to the nearby grain interiors. Elemental distribution results, gained through a comparison of the STEM EELS quantification data recorded at different regions, suggest the enrichment of La at grain boundaries or triple junctions in contrast to its shortage in the adjacent parts. This is in agreement with the aforementioned STEM EDX results. Specifically, the enhanced concentrations of Gd at grain boundaries indicate the segregation of Gd, which is consistent with the previous observation about the Gd aggregation/segregation at grain boundaries in doped ceria [13]. Moreover, the enrichment of both La and Gd mainly at grain boundaries further verifies the preference of dopants or impurities to segregate at boundary region. It is thereby reasonable to draw the inference that the La, mainly detected at grain boundaries or triple junctions at the GDC region, transfers from the cathode side in the form of diffusing along grain boundaries. It is believed that the A cation in ABO_3 perovskite has relatively higher mobility and La is also a mobile element [15]. Additionally, due to the similarity between La and Ce, a broad solubility range can be expected between La and ceria. These can accordingly explain the phenomenon that, only the element La is mainly detected in LSCF at grain boundaries or triple junctions. It is hence attested that grain boundaries can provide another pathway for elements diffusion around the interfacial region. This also can be interpreted with the widely accepted principle that grain boundaries can provide accommodation/volume for aggregation/segregation of dopants, diffusing elements and other impurities, or possible channels for mass transport [16].

Table 1
Quantification results of STEM EELS acquired at different positions.

	Ce (at%)	Gd (at%)	La (at%)
G1	78.09 ± 7.6	21.91 ± 3.4	0 ± 0.4
G2	74.70 ± 6.4	25.30 ± 6.3	0 ± 0.5
GB1	59.23 ± 6.9	36.73 ± 5.2	4.04 ± 0.4
TJ2	54.97 ± 6.5	40.79 ± 6.1	4.24 ± 0.7
TJ1	52.73 ± 6.4	37.93 ± 4.6	9.35 ± 0.7

4. Conclusions

To summarize, the microstructures, related chemical composition, electronic state and spatial concentration of constituent elements at the cathode/electrolyte interface, have been investigated by means of a combination of various techniques, namely SEM, TEM, HAADF, EDX and EELS operated in STEM mode. Two types of diffusions, mutual diffusion and diffusion along grain boundaries have been clarified at the cathode/electrolyte interface. STEM EDX analyses illustrate mutual diffusions in which all cations in LSCF and GDC substitutionally diffuse into each other. It is verified that such mutual diffusion is independent of the ionic radius of diffusing cations. Besides, this study also manifests through quantifying STEM EELS spectra that elements in the cathode can diffuse into the electrode along grain boundaries in the vicinity of the cathode/electrolyte interface, and subsequently segregate at grain boundaries or triple junctions. It is noteworthy that these two types of diffusions, i.e. the mutual diffusion and diffusion along grain boundaries, actually occur before the cells are operated. Consequently, it draws much attention to cell sample preparation in order to fabricate high quality electrolyte/electrode interfaces for IT-SOFC applications.

Acknowledgments

This research was founded by the Grant-in-Aid for Scientific Research (22310053) of the Ministry of Education, Culture, Sports, and Technology (MEXT), Japan. The authors also gratefully acknowledges the partial financial support of the Global Research center for Environment and Energy based on Nanomaterials science (GREEN), National Institute for Materials Science, Japan.

References

[1] B.C.H. Steele, A. Heinzel, Nature 414 (2001) 345.
[2] T. Suzuki, Z. Hasan, Y. Funahashi, T. Yamaguchi, Y. Fujishiro, M. Awano, Science 325 (2009) 852.
[3] J.A.M. Roosmalen, E.H.P. Cordfunke, Solid State Ionics 52 (1992) 303.
[4] A. Tsoga, A. Gupta, A. Naoumidis, P. Nikolopoulos, Acta Mater. 48 (2000) 4709.
[5] N. Sakia, H. Kishimoto, K. Yamaji, T. Horita, M.E. Brito, H. Yokokawa, J. Electrochem. Soc. 154 (2007) B1331.
[6] A. Mai, V.A.C. Haanappel, F. Tietz, D. Stover, Solid State Ionics 177 (2006) 2103.
[7] D. Waller, J.A. Lane, J.A. Kilner, B.C.H. Steele, Solid State Ionics 86 (1996) 767.
[8] Y. Leng, S.H. Chan, Q. Liu, Int. J. Hydrogen Energy 33 (2008) 3808.
[9] R. Knibbe, J. Hjelm, M. Menon, N. Pryds, M. Sogaard, H.J. Wang, K. Neufeld, J. Am. Ceram. Soc. 93 (2010) 2877.
[10] Z.P. Li, T. Mori, G.J. Auchterlonie, Y.N. Guo, J. Zou, J. Drennan, M. Miyayam, J. Phys. Chem. C 115 (2011) 6877.
[11] Z.P. Li, T. Mori, G.J. Auchterlonie, J. Zou, J. Drennan, M. Miyayama, Solid State Ionics 191 (2011) 55.
[12] D.R. Ou, T. Mori, F. Ye, M. Miyayama, S. Nakayama, J. Zou, G.J. Auchterlonie, J. Drennan, J. Electrochem. Soc. 156 (2009) B825.
[13] Z.P. Li, T. Mori, G. Auchterlonie, J. Zou, J. Drennan, Appl. Phys. Lett. 98 (2011) 093104.
[14] E. Konysheva, J.T.S. Irvine, A. Besmehn, Solid State Ionics 180 (2009) 778.
[15] W. Zajac, K. Swierczek, J. Molenda, J. Power Sources 173 (2007) 675.
[16] M.P. Seah, J. Phys. F: Metal Phys. 10 (1980) 1043.